Check for updates

Anion effects on Li ion transference number and dynamic ion correlations in glyme–Li salt equimolar mixtures†

Keisuke Shigenobu,[a] Masayuki Shibata,[b] Kaoru Dokko, [ID] [ac]
Masayoshi Watanabe, [ID] [c] Kenta Fujii [ID] *[b] and Kazuhide Ueno [ID] *[ac]

To achieve single-ion conducting liquid electrolytes for the rapid charge and discharge of Li secondary batteries, improvement in the Li$^+$ transference number of the electrolytes is integral. Few studies have established a feasible design for achieving Li$^+$ transference numbers approaching unity in liquid electrolytes consisting of low-molecular-weight salts and solvents. Previously, we studied the effects of Li$^+$–solvent interactions on the Li$^+$ transference number in glyme- and sulfolane-based molten Li salt solvates and clarified the relationship between this transference number and correlated ion motions. In this study, to deepen our insight into the design principles of single-ion conducting liquid electrolytes, we focused on the effects of Li$^+$–anion interactions on Li ion transport in glyme–Li salt equimolar mixtures with different counter anions. Interestingly, the equimolar triglyme (G3)–lithium trifluoroacetate (Li[TFA]) mixture ([Li(G3)][TFA]) demonstrated a high Li$^+$ transference number, estimated *via* the potentiostatic polarization method (t_{Li}^{PP} = 0.90). Dynamic ion correlation studies suggested that the high t_{Li}^{PP} could be mainly ascribed to the strongly coupled Li$^+$–anion motions in the electrolytes. Furthermore, high-energy X-ray total scattering measurements combined with all-atom molecular dynamics simulations showed that Li$^+$ ions and [TFA] anions aggregated into ionic clusters with a relatively long-range ion-ordered structure. Therefore, the collective motions of the Li ions and anions in the form of highly aggregated ion clusters, which likely diminish rather than enhance ionic conductivity, play a significant role in achieving high t_{Li}^{PP} in liquid electrolytes. Based on the dynamic ion correlations, a potential design approach is discussed to accomplish single-ion conducting liquid electrolytes with high ionic conductivity.

1. Introduction

The feasibility of achieving rapid charge and discharge capabilities in Li secondary batteries has spurred significant interest in

[a] *Department of Chemistry and Life Science, Yokohama National University, 79-5 Tokiwadai, Hodogaya-ku, Yokohama 240-8501, Japan. E-mail: ueno-kazuhide-rc@ynu.ac.jp; Fax: +81-45-339-3951; Tel: +81-45-339-3951*

[b] *Graduate School of Sciences and Technology for Innovation, Yamaguchi University, 2-16-1 Tokiwadai, Ube, Yamaguchi 755-8611, Japan E-mail: k-fujii@yamaguchi-u.ac.jp; Fax: +81-836-85-9212; Tel: +81-836-85-9212*

[c] *Advanced Chemical Energy Research Centre (ACERC), Institute of Advanced Sciences, Yokohama National University, 79-5 Tokiwadai, Hodogaya-ku, Yokohama 240-8501, Japan*

† Electronic supplementary information (ESI) available: Plots of the Li/Li$^+$ electrode potential against the natural logarithm of the Li salt concentration in the mixture of LiX in glyme (G3 or G4); the product of t_{Li}^{PP} and σ_{ion} *versus* ionicity; X-ray structure factors $S(q)$ and corresponding radial distribution functions in the form of $[r^2[G(r) - 1]]$s; snapshot of the coordination structure of $[Li_2(G3)_2]^{2+}$; Li$^+$–Li$^+$ pair correlation function $[g_{Li–Li}^{MD}(r)$ for [Li(G3)][TFSA]; numerical data for the composition of the systems and density values; force field parameters; the six experimentally obtained parameters for the calculation of the Onsager and normalized transport coefficients; Li–Li distances obtained from the crystal structure of Li[TFA] and G4 mixture. See DOI: 10.1039/d0cp06381a

enhancing Li$^+$ ion transport properties, including the ionic conductivity and Li$^+$ transference number of liquid electrolytes.[1–3] In general, the ionic conductivity of the electrolyte is believed to be the most important parameter for improving the rapid charge/discharge ability, and many studies have focused on enhancing the ionic conductivity of electrolyte materials. Liquid electrolytes with a salt concentration of ∼1 mol dm^{-3} are usually employed for battery applications because of their maximum conductivity in this concentration range. Over the past decade, however, highly concentrated electrolytes including molten Li salt solvates have captured significant attention owing to their unique electrochemical, physicochemical, and thermal properties, despite their low ionic conductivity. Li secondary batteries using concentrated liquid electrolytes have demonstrated improved rate capability, long-term cycling, and high coulombic efficiency.[4–7] The unique cation transport decoupled from viscosity and the relatively high cationic transference number of the concentrated electrolytes have been considered as possible reasons for the improved rate capability.[8–10]

In the design of liquid electrolytes with high Li$^+$ transport properties, the enhancement of the Li$^+$ transference number remains challenging. Indeed, few studies have undertaken a

2622 | *Phys. Chem. Chem. Phys.*, 2021, **23**, 2622–2629

This journal is © the Owner Societies 2021

profound analysis of the Li$^+$ transference number, although this parameter has often been used to discuss the rapid charge and discharge capability.[11] The literature values of Li$^+$ transference numbers have been summarized and discussed for carbonate-based organic electrolyte solutions,[12,13] and the anion dependence of the Li$^+$ transference number has been studied for organic[14,15] and polymer electrolytes.[16–19] To deepen our fundamental understanding of Li ion conduction along with the Li$^+$ transference number, we previously investigated solvent effects on the Li$^+$ transference number for molten Li salt solvates of lithium bis(trifluoromethanesulfonyl)amide (Li[TFSA]) with glymes (CH$_3$O(CH$_2$CH$_2$O)$_n$CH, Gn) and sulfolane (SL) and their relationship with ion cross-correlations (cation–cation, anion–anion, and cation–anion) based on the Onsager reciprocal relations.[20] We found that the extremely low Li$^+$ transference number (0.028) of [Li(G4)][TFSA], estimated *via* the potentiostatic polarization, was predominantly caused by the anti-correlated cation–cation motions of crown-ether-like, robust [Li(G4)]$^+$ complex cations, while the relatively high Li$^+$ transference number ($\sim$0.7) of SL-based molten Li salt solvates was ascribed to weaker anti-correlations of cation–cation and cation–anion motions in a unique SL-bridged Li$^+$ ion coordination structure. Thus, these different ion–solvent interactions and ion correlations in the electrolytes are crucial determinants for the Li$^+$ transference number.

The interaction between Li$^+$ ions and counter anions is also a key factor governing the Li$^+$ ion coordination structure and Li$^+$ transport properties. In a previous study, the effects of Li$^+$–anion interactions on the stability of the complex cation and ionic transport properties of the glyme–Li salt equimolar mixtures with different Li salts ([Li(glyme)]X) were systematically studied.[21] Robust [Li(glyme)]$^+$ complex cations were formed only with weakly coordinating, bulky anions (such as [TFSA]), while the glyme molecules remained uncoordinated to some extent in [Li(glyme)]X with strongly Lewis basic anions. [Li(glyme)]X with dissociative perfluorinated sulfonylamide anions (such as [TFSA]) showed higher ionic conductivities and apparent dissociation degrees (or ionicities) than [Li(glyme)]X with more Lewis basic anions.

Herein, we report the effects of Li$^+$–anion interactions on the Li$^+$ transference number of [Li(glyme)]X, for X ranging from weakly coordinating anions (such as [TFSA]) to moderately basic anions (such as trifluoromethanesulfonate ([TfO], BF$_4$, and ClO$_4$) to strongly Lewis basic anions (such as NO$_3$ and trifluoroacetate [TFA]). The anion dependence of the Li$^+$ ion transport mechanism is further discussed in the context of dynamic ion correlations based on Roling and Bedrov's concentrated solution theory.[22] Finally, we conducted high-energy X-ray total scattering (HEXTS) experiments combined with all-atom molecular dynamics (MD) simulations to clarify the relationship between the dynamic ion correlations and solution structures in the equimolar glyme–Li salt mixtures.

2. Experimental

2.1 Materials

Purified triglyme (G3) and tetraglyme (G4) were kindly supplied by Nippon Nyukazai Co. (Japan). Lithium bis(trifluoromethanesulfonyl)amide

(Li[TFSA]) was kindly provided by Solvay Japan. Battery-grade Li salts–lithium bis(fluorosulfonyl)amide (Li[FSA]), lithium bis(pentafluoroethanesulfonyl)amide (Li[BETA]), lithium trifluoromethanesulfonate (Li[TfO]), LiBF$_4$, and LiClO$_4$—were purchased from Kishida Chemical Co. (Japan). The other Li salts–lithium bis(nonafluorobutanesulfonyl)amide (Li[NFSA]), lithium trifluoroacetate (Li[TFA]) and LiNO$_3$—were obtained from Mitsubishi Materials Electronic Chemicals Co. (Japan), Alfa Aesar and FUJIFILM Wako Pure Chemical Co. (Japan), respectively. All glyme–Li salt mixtures were prepared in an inert argon-filled glove box ([H$_2$O] < 1 ppm; [O$_2$] < 1 ppm).

2.2 Measurements

The experiments to determine two different Li$^+$ transference numbers (t_{Li}^{NMR} and t_{Li}^{PP}), the salt diffusion coefficients, and electrode potentials of Li/Li$^+$ conducted in this study were performed according to our previous report.[20] In brief, for the Li$^+$ transference number determined by the potentiostatic polarization method (t_{Li}^{PP}), experiments were performed using a Li symmetric cell. A porous glass filter paper (Advantec, GA55, 17 mm in diameter) or two pieces of microporous propylene membrane separator (Celgard, Celgard3501, 17 mm in diameter) soaked in the liquid electrolyte were inserted into two Li foil electrodes (Honjo Metal, 16 mm in diameter) in a 2032 coin-type cell. Impedance spectra were measured in the frequency range of 100 mHz–1 MHz with a voltage amplitude of 10 mV using a potentiostat (Solartron Analytical, ModuLab XM ECS). The salt diffusion coefficients (D_{salt}) were determined using the same Li symmetric coin cell according to the literature.[23] The cell was polarized at 10 mV in potentiostatic mode and the relaxation of the cell potential was recorded after the applied potential was removed. D_{salt} was determined by fitting the potential relaxation with a single exponential decay function. The electrode potentials of Li/Li$^+$ ($\Delta\varphi$) were measured *via* a reference electrode (Li/Li$^+$ in 1 mol dm^{-3} Li[TFSA]/G3) using a multi-compartment concentration cell (Fig. S1, ESI†).[24] Vycor glass was used for the junction between the reference electrolyte and the sample electrolytes. The potential was recorded using a potentiostat. A slope d$\Delta\varphi$/d ln(c) at a given concentration was obtained from the slope of the concentration dependence of the concentration cell potential.[22] All the above measurements were performed at 30 °C unless otherwise noted.

High-energy X-ray total scattering measurements for the electrolytes were conducted at ambient temperature using an X-ray diffraction apparatus[25] (BL04B2 beamline at SPring-8, JASRI, Japan). Monochrome 61.6 keV X-rays were obtained using a Si(220) monochromator. The observed X-ray scattering intensities were corrected for adsorption, polarization, and incoherent scattering to obtain coherent scattering intensities, $I_{coh}(q)$.[26–28]

The X-ray structure factor $S^{HEXTS}(q)$ per stoichiometric volume was expressed as follows:

$$S^{HEXTS}(q) = \frac{\frac{I_{coh}(q)}{N} - \sum n_i f_i(q)^2}{\{\sum n_i f_i(q)\}^2} + 1 \qquad (1)$$

This journal is © the Owner Societies 2021

Phys. Chem. Chem. Phys., 2021, **23**, 2622–2629 | **2623**

where n_i and $f_i(q)$ correspond to the number and atomic scattering factor of atom i, respectively. The X-ray radial distribution function $G^{HEXTS}(q)$ was calculated from the inverse Fourier transform of $S^{HEXTS}(q)$:

$$G^{exp}(r) - 1 = \frac{1}{2\pi^2 r \rho_0} \int_0^{q_{max}} q[S^{exp}(q) - 1] \sin(qr) \frac{\sin(q\pi/q_{max})}{q\pi/q_{max}} dq \tag{2}$$

where ρ_0 corresponds to the number density of atoms and q_{max} represents the maximum value of q (= 25 Å^{-1} in this study).

2.3 MD simulations

The MD simulations were performed with the GROMACS 2016.5 program under the *NTP* ensemble condition controlled by the Nosé–Hoover thermostat[29,30] (at 298 K and 1 atm). To ensure the random starting configuration, firstly, we mixed Li$^+$ [TFA]$^-$ and G3 molecules at high temperature and pressure (1000 K and 1000 atm, respectively) for 1 ns. The composition (*i.e.*, the number of Li[TFSA] and Li[TFA] ion pairs, respectively, and G3 molecules) in a cubic cell was as follows: Li[TFSA]/G3 = 790/790 and Li[TFA]/G3 = 790/790. The resulting box size and density at the equilibrium state are listed in Table S1 (ESI†). The total simulation time was set as 15.0 ns for both systems. The X-ray weighted structure factors $S^{MD}(q)$ and radial distribution functions $G^{MD}(q)$ were obtained by analyzing the data collected at 0.1 ps intervals during the last 500 ps. CLaP and OPLS-AA force fields, including intermolecular Lennard-Jones (LJ) and coulombic interactions and intramolecular interactions with (1) bond stretching, (2) angle bending, and (3) torsion of dihedral angles, were used for [TFSA],[31] [TFA][32−34] and G3.[32,33,35] The LJ parameter for Li ions (see the Li salt/ carbonate solvent system[36]) was used. The partial charges (q^+ and q^-) for TFA molecules (Fig. S2, ESI†) were obtained from quantum chemical calculations (ChelpG method[37]); the resulting values are listed in Table S2 (ESI†). Those for TFSA and G3 were similar to the values reported in a previous work.[38]

The $S^{MD}(q)$ functions were calculated using the trajectories from the MD simulations as follows:

$$S^{MD}(q) =$$

$$\begin{cases} \dfrac{\sum_i \sum_j \left\{ \dfrac{n_i(n_j-1)f_i(q)f_j(q)}{N(N-1)} \right\}}{\left\{ \sum_k \left(\dfrac{n_k f_k(q)}{N} \right) \right\}^2} \int_0^r 4\pi^2 \rho_0 \left(g_{ij}^{MD}(r) - 1 \right) \dfrac{\sin qr}{qr} dr + 1 \quad (i = j) \\[4ex] \dfrac{\sum_i \sum_j \left\{ \dfrac{2n_i n_j f_i(q)f_j(q)}{N^2} \right\}}{\left\{ \sum_k \left(\dfrac{n_k f_k(q)}{N} \right) \right\}^2} \int_0^r 4\pi^2 \rho_0 \left(g_{ij}^{MD}(r) - 1 \right) \dfrac{\sin qr}{qr} dr + 1 \quad (i \neq j) \end{cases} \tag{3}$$

where N is the total number of atoms in the simulation box defined by $N = \sum_k n_k$, and $g_{ij}^{MD}(r)$ is the atom–atom pair correlation function between atoms i and j. The $G^{MD}(q)$ functions were calculated from

the corresponding $S^{MD}(q)$s, conducting a similar procedure to that of HEXTS.

3. Results and discussion

3.1 Li$^+$ transference number under anion-blocking condition

In our previous work, Li$^+$ transference numbers derived from the pulsed filed gradient (PFG)-NMR method (t_{Li}^{NMR}) and potentiostatic polarization method (t_{Li}^{PP}) were determined for Li-ion conducting electrolytes.[21,39,40] The PFG-NMR method is based on the Nernst–Einstein equation: $t_{Li}^{NMR} = D_{Li}/(D_{Li} + D_{anion})$, where D_{Li} and D_{anion} are the self-diffusion coefficients of Li$^+$ ions and anions, respectively, and the ions are assumed to be completely dissociated and move independently as ideal dilute electrolyte solutions. Hence, for highly concentrated electrolytes, t_{Li}^{NMR} would not reflect a realistic transference number because of their dynamic ion correlations.

The Li$^+$ transference number based on the potentiostatic polarization combined with electrochemical impedance spectroscopy[41,42] (t_{Li}^{PP}) is defined as follows:

$$t_{Li}^{PP} = \frac{I_{SS}(V_{DC} - I_{Ohm}R_{i,0})}{I_{Ohm}(V_{DC} - I_{SS}R_{i,SS})} \tag{4}$$

where V_{DC} is a constant applied voltage, I_{Ohm} and I_{SS} are the initial and steady-state currents, and $R_{i,0}$ and $R_{i,SS}$ are the initial and steady-state interfacial resistance values, respectively. The initial current is calculated using Ohm's law, $I_{Ohm} = V_{DC}/(R_{bulk} + R_{i,0})$, because the "measured" initial current data point (I_0) strongly depends on the sampling time, which results in the inaccurate determination of t_{Li}^{PP} in some cases. Similar to t_{Li}^{NMR}, t_{Li}^{PP} represents the precise Li$^+$ transference number only for ideal dilute electrolyte solutions. According to Balsara *et al.*,[43] t_{Li}^{PP} simply shows the "current fraction" in non-ideal electrolytes; however, t_{Li}^{PP} is convenient for assessing Li$^+$ transport properties because the value includes migration and diffusion effects, which would also be observed in lithium ion batteries (under anion-blocking conditions).

Fig. 1(a) shows the t_{Li}^{PP} of the glyme–Li salt equimolar mixtures plotted as a function of ionicity. Ionicity, defined as the molar conductivity ratio (Λ/Λ_{NE}), expresses the extent to which the self-diffusion of ionic species contributes to the actual ionic conduction and is relevant to the apparent degree of dissociation or dynamic ion correlations in electrolyte solutions.[39,44−48] Λ is the experimental molar conductivity and Λ_{NE} is calculated from self-diffusion coefficients using the Nernst–Einstein equation, $\Lambda_{NE} = F^2(D_{Li} + D_{anion})/RT$, where F is the Faraday constant, R is the gas constant, and T is the absolute temperature. As noted in previous papers,[21,49] the strength order of Lewis basicity for the selected ions is [TFSA] < ClO$_4$ < BF$_4$ < [TfO] < NO$_3$ < [TFA], whereas their order of ionicity in [Li(glyme)]X displays the exact opposite trend.

Interestingly, a good linear relationship is observed between t_{Li}^{PP} and ionicity (Fig. 1(a)). [Li(glyme)]X with weakly coordinating anions such as the bis(perfluorosulfonyl)amides ([FSA], [TFSA], [BETA], [NFSA]) and ClO$_4$ show significantly low t_{Li}^{PP} values of less

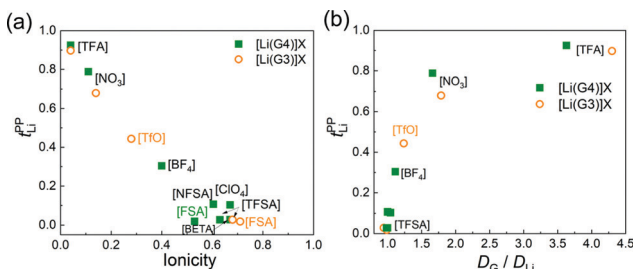**Fig. 1** Relationships between (a) t_{Li}^{PP} and ionicity, and (b) t_{Li}^{PP} and D_G/D_{Li} for [Li(glyme)]X. Ionicity and D_G/D_{Li} values were obtained from ref. 21.

Fig. 2 Plots of t_{Li}^{PP} versus ionic conductivity for [Li(glyme)]X.

than 0.1. The value of t_{Li}^{PP} increases with decreasing ionicity (i.e., increasing Lewis basicity of the anions). The highest value of t_{Li}^{PP} is 0.93 for [Li(G4)][TFA], with the lowest ionicity of 0.04, whereas the lowest t_{Li}^{PP} value of 0.016 is observed for [Li(G3)][FSA], with the highest ionicity of 0.71. In Fig. 1(b), t_{Li}^{PP} values are plotted against the ratios of the self-diffusion coefficients of the glyme and Li$^+$ ions (D_G/D_{Li}). Here, D_G/D_{Li} reflects the stability of [Li(glyme)]$^+$ complex ions in the equimolar glyme–Li salt mixtures.[21] $D_G/D_{Li} \approx 1$ (for [Li(glyme)]X with weakly coordinating anions, such as [Li(G3)][TFSA]) indicates the coupled diffusion of the glyme and Li$^+$ ions in the form of [Li(glyme)]$^+$ complex ions. In contrast, if $D_G/D_{Li} > 1$ (for [Li(glyme)]X with strongly Lewis basic anions, such as [Li(G3)][TFA]), the complex ions are considered to be short-lived or unstable, and the glymes remain uncoordinated to some extent in the equimolar glyme–Li salt mixtures.

The anion-dependent stability of [Li(glyme)]$^+$ complex ions was also evaluated in light of the Li$^+$–glyme residence time using MD simulations.[50] The residence time of the Li$^+$–glyme complex was much shorter than that of the Li$^+$–anion pair for the glyme–Li salt mixtures with strongly Lewis basic anions (such as [TFA]). As a consequence of strong Li$^+$–anion interactions, uncoordinated glymes and Li$^+$–anion pairs mainly comprise the glyme–Li salt mixtures with Lewis basic anions. Therefore, the presence of uncoordinated (or highly exchangeable) glymes and/or Li$^+$–anion pairs is suggested to be responsible for the high t_{Li}^{PP} values of [Li(glyme)]X with strongly Lewis basic anions. MD simulations by Bedrov et al. demonstrated that the enhancement of the Li$^+$ transference number under anion-blocking conditions is attributable to the reduction of Li$^+$–solvent residence time by shortening the chain length of the glymes.[22] In this regard, our results shown in Fig. 1(b) are in good agreement with their notion: the presence of free (or highly exchangeable) glyme, which is accompanied by strong Li$^+$–anion interactions in the present system, results in high t_{Li}^{PP} values.

The relationship between t_{Li}^{PP} and the ionic conductivity of [Li(glyme)]X is illustrated in Fig. 2. The lowest ionic conductivity of 0.083 mS cm^{-1} is observed for [Li(G4)][TFA], with the highest t_{Li}^{PP} value of 0.93, whereas the highest ionic conductivity of 1.7 mS cm^{-1} is achieved for [Li(G3)][FSA], with the lowest t_{Li}^{PP} value of 0.016. The figure clearly indicates that more Lewis basic anions contribute to the enhancement of t_{Li}^{PP}, while decreasing the ionic conductivity. Balsara et al. confirmed a similar "trade-off" between the Li$^+$ transference number and ionic conductivity for Li$^+$ ion-conducting solid polymer electrolytes.[43] The Li$^+$ ionic
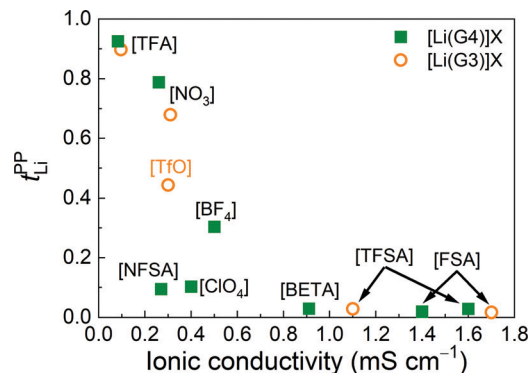
conductivity characterized by the product of t_{Li}^{PP} and the conductivity is larger for [Li(glyme)]X with NO$_3$, [TfO] and BF$_4$ anions than [Li(glyme)]X with strongly Lewis basic [TFA] and weakly coordinating anions such as [FSA] (see Fig. S3, ESI†). Thus, higher Li$^+$ transport properties can be achieved with the moderately basic anions. In the following sections, we investigate the causes underlying the enhancement of t_{Li}^{PP} for strongly Lewis basic anions and the inverse relationship between t_{Li}^{PP} and ionic conductivity from the viewpoint of dynamic ion correlations and liquid structures.

3.2 Dynamic ion correlations

For aqueous electrolyte solutions, dynamic ion correlations were systematically evaluated based on the velocity cross-correlation functions by Woolf and Harris.[51,52] For solid polymer electrolytes, recently, Balsara and Newman investigated the correlations by introducing the Stefan–Maxwell diffusion coefficients.[43,53,54] Regarding non-aqueous liquid electrolyte solutions, dynamic ion correlations were derived from the Onsager transport coefficients and were first applied for the glyme molten Li salt solvates of Li[TFSA] by Roling and Bedrov et al.[22,55,56] In our previous work, we discussed transport behavior in glyme- and SL-based molten Li salt solvates by introducing experimentally determined transport coefficients. The Onsager transport coefficients can describe the ionic conductivity σ_{ion} as follows:

$$\sigma_{ion} = \sigma_{++} + \sigma_{--} - 2\sigma_{+-} \quad (5)$$

Here, σ_{++} and σ_{--} consist of self-terms and distinct terms, respectively, and the ionic conductivity σ_{ion} is expressed as

$$\sigma_{ion} = \sigma_+^{self} + \sigma_{++}^{distinct} + \sigma_-^{self} + \sigma_{--}^{distinct} - 2\sigma_{+-}. \quad (6)$$

All the Onsager transport coefficients (σ_{++}, σ_{--}, and σ_{+-}) can be calculated from four experimental quantities—σ_{ion}, t_{Li}^{PP}, D_{salt}, and $d\Delta\varphi/d\ln(c)$; these data are shown in Table S3 (ESI†). The detailed procedure for estimating the transport coefficients was described in a previous paper.[20] The dynamic cross-correlations of the ions (cation–cation, anion–anion, cation–anion) are indicated by the signs of $\sigma_{++}^{distinct}$, $\sigma_{--}^{distinct}$, and σ_{+-}, respectively. The sign of the cross-correlation is positive in the case of correlated ion motions, while the sign is negative for anti-correlated

This journal is © the Owner Societies 2021

Phys. Chem. Chem. Phys., 2021, **23**, 2622–2629 | **2625**

motions. In addition, a value of zero for these correlations indicates non-correlated interionic dynamics, as predicted in ideal electrolyte solutions.

To clarify the effects of the interionic dynamics on the anionic dependency of t_{Li}^{PP} and the trade-off between t_{Li}^{PP} and ionic conductivity, the ion dynamics for the extraordinary case of [Li(G3)][TFA] was compared with those of another extreme case, [Li(G3)][TFSA], reported in our prior study.[20] As discussed in the previous section, both glyme–Li salt mixtures show exactly opposite properties: [Li(G3)][TFA] shows high t_{Li}^{PP} but poor ionic conductivity, and [Li(G3)][TFSA] displays high ionic conductivity but very low t_{Li}^{PP}.

The normalized Onsager transport coefficients (σ_+^{self}, σ_-^{self}, $\sigma_{++}^{distinct}$, $\sigma_{--}^{distinct}$, and σ_{+-} divided by σ_{ion}) of [Li(G3)][TFA] are shown in Fig. 3(a), and the numerical data are listed in Table S4 (ESI†). Interestingly, all five coefficients ($\sigma_+^{self}/\sigma_{ion}$, $\sigma_-^{self}/\sigma_{ion}$, $\sigma_{++}^{distinct}/\sigma_{ion}$, $\sigma_{--}^{distinct}/\sigma_{ion}$, and σ_{+-}/σ_{ion}) are positive for [Li(G3)][TFA]. This is distinctly different from the results for the previously studied [Li(G3)][TFSA], for which $\sigma_{++}^{distinct}/\sigma_{ion}$, $\sigma_{--}^{distinct}/\sigma_{ion}$, and σ_{+-}/σ_{ion} were all negative.[20] Fig. 3(b) depicts the σ_{+-}/σ_{ion} values for [Li(G3)][TFSA], [Li(G4)][BF$_4$], and [Li(G3)][TfO]. σ_{+-}/σ_{ion} shifts from a negative value for [Li(G3)][TFSA] to moderately positive values for [Li(G4)][BF$_4$] and [Li(G3)][TfO], and a largely positive value for [Li(G3)][TFA] (Fig. 3(a)), confirming that the σ_{+-}/σ_{ion} value is reflective of the Li$^+$–anion interactions in [Li(glyme)]X.

The correlated motions of the ion species with the same sign contribute to the enhancement of the ionic conductivity; however, the correlated motions of the cation–anion negatively affect the ionic conductivity. Thus, the correlated cation–anion motions almost offset the positive contribution from σ_+^{self}, σ_-^{self}, $\sigma_{++}^{distinct}$, and $\sigma_{--}^{distinct}$ to the ionic conductivity; therefore, [Li(G3)][TFA] exhibits very low ionic conductivity among the glyme–Li salt mixtures studied here.

In addition, the normalized values of the five Onsager transport coefficients for [Li(G3)][TFA] (Fig. 3(a)) are nearly hundreds of times larger than those of [Li(G3)][TFSA] simply because of its low ionic conductivity. The calculation of the five transport coefficients is affected by the self-diffusion coefficients determined for Li$^+$ and the anions. The larger values of the normalized coefficients suggest that the measured self-diffusion coefficients of the ions in [Li(G3)][TFA] contribute little to the actual ionic conductivity (σ_{ion}). The largely positive

values of $\sigma_{++}^{distinct}/\sigma_{ion}$, $\sigma_{--}^{distinct}/\sigma_{ion}$, and σ_{+-}/σ_{ion} for [Li(G3)][TFA] (Fig. 3(a)) suggest that all of the ions tend to move preferentially in the same direction. These results raise the possibility that Li$^+$ ions and [TFA] anions form ionic aggregates or ion clusters of $[Li_x^+([TFA]^-)_y]^{(x-y)}$ as well as neutral ion pairs of Li–[TFA].

3.3 Liquid structures

The solution structures of [Li(G3)][TFA] and [Li(G3)][TFSA] were investigated HEXTS and all-atom MD simulations. Fig. S4 (ESI†) shows the X-ray structure factors, $S(q)$s, obtained from HEXTS and MD simulations within the q range of 0–20 Å. In addition, Fig. S5 (ESI†) illustrates the corresponding X-ray radial distribution functions, $r^2\{G(r) - 1\}$, in the r range of 0–25 Å. In both cases, the $S(q)$s and corresponding $[r^2\{G(r) - 1\}]$s obtained from the MD simulations reproduce the HEXTS profiles accurately. Therefore, we can further consider the coordination structures and intramolecular/intermolecular interactions through analysis of MD simulations. It is possible to transform the $[r^2\{G(r) - 1\}]$s into atom–atom pair correlation functions for each component. The correlation functions of the Li$^+$–Li$^+$ and Li$^+$–anions are depicted in Fig. 4.

Fig. 4(a) shows the atom–atom pair correlation function (g) between the Li ions of [Li(G3)][TFSA] and [Li(G3)][TFA]. Regarding [Li(G3)][TFSA], two sharp peaks appear at 3.0 and 9.2 Å, corresponding to the $[g_{Li-Li}^{MD}(r)]$ for Li$^+$–glyme complexes. The first peak can be assigned to the Li$^+$–Li$^+$ correlation, which is attributable to the two Li ions coordinated with same G3 molecule, suggesting the formation of dimers such as $[Li_2(G3)_2]^{2+}$ in this electrolyte (Fig. S6, ESI†); however, because the cumulative coordination number ($N(r)$) is lower than 0.15 (see Fig. S7, ESI†), the existence probability of this structure is low. The second peak (9.2 Å) can be attributed to a correlation between $[Li(G3)]^+$ complexes. This result is strongly supported by the previous study for [Li(G4)][TFSA].[35] The potential mean force (PMF) for the Li$^+$–Li$^+$ pair correlation (PMF = $-RT \ln g_{Li-Li}^{MD}(r)$) of [Li(G4)][TFSA] has a minimum value at 9.5 Å, suggesting that stable $[Li(G4)]^+$ complex cations predominantly exist by maintaining the distance between the other complex cations.[35]

In contrast, multiple sharp peaks appear in the correlation function for [Li(G3)][TFA]. These peaks start to emerge at 3.8 Å and continue until 12.8 Å with nearly regular intervals between peaks. This strongly suggests that the Li$^+$–Li$^+$ correlation in
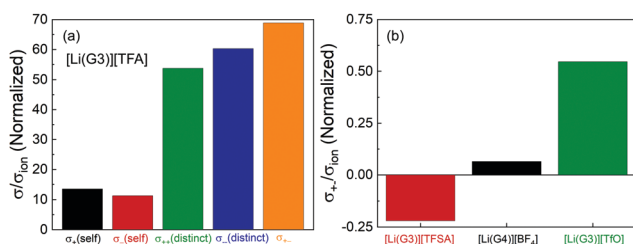

Fig. 3 (a) All Onsager transport coefficients (σ_+^{self}, σ_-^{self}, $\sigma_{++}^{distinct}$, $\sigma_{--}^{distinct}$ and σ_{+-}: left to right) normalized by σ_{ion} of [Li(G3)][TFA], and (b) differences in σ_{+-} (cross-correlation of cation–anion) of several G3- or G4-based glyme–Li salt equimolar mixtures.

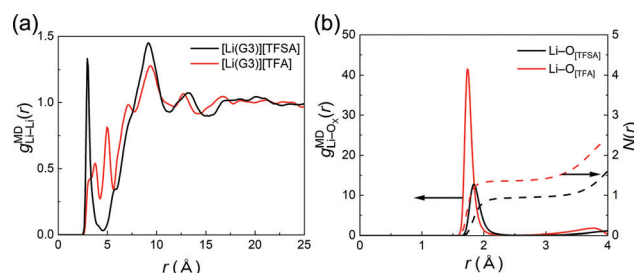**Fig. 4** Atom–atom pair correlation functions $[g_{atom-atom}^{MD}(r)]$s between (a) Li-ions and (b) for the O atoms of anions around Li ions and integrated profiles (cumulative coordination number: $N(r)$) for [Li(G3)][TFSA] and [Li(G3)][TFA].
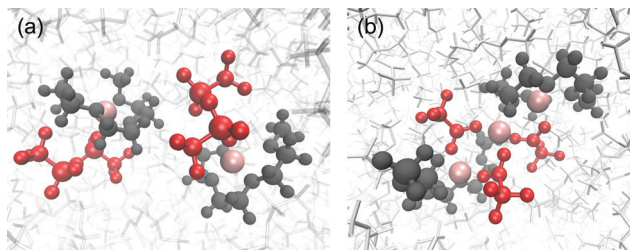
2626 | *Phys. Chem. Chem. Phys.*, 2021, **23**, 2622–2629

This journal is © the Owner Societies 2021

Fig. 5 Snapshots of the coordination structures found in (a) [Li(G3)][TFSA] and (b) [Li(G3)][TFA] obtained from MD simulations. Pink: Li⁺, red: anions and dark grey: G3.

[Li(G3)][TFA] can be ascribed not only to Li⁺–solvent (G3) inter-actions but also to Li⁺–anion interactions, and a continuous Li⁺-ordered structure is formed as a polynuclear complex over a relatively long distance. Similar long-range ion-ordering was also observed in a highly concentrated electrolyte of Li[TFSA] in *N*,*N*-dimethylformamide.[57] Fig. 4(b) shows the Li⁺–anion pair correlations and the integrated profile (cumulative coordination number: $N(r)$) for each electrolyte, where the distance for the correlations of Li⁺–[TFA] anions is shorter than that of Li⁺–[TFSA]. In addition, the intensity of the peak for the Li⁺–[TFA] anion correlation is four times larger and the shape of the peak is much sharper. Moreover, the cumulative number of Li⁺–[TFA] anions is much higher than that of Li⁺–[TFSA]. These findings are consistent with the solution structure presumed from the dynamic ion correlations of [Li(G3)][TFA] investigated in the previous section: [TFA] anions strongly interact with Li⁺, and the aggregating structure is dominant in [Li(G3)][TFA].

Snapshots of the coordination structures of [Li(G3)][TFSA] and [Li(G3)][TFA] are presented in Fig. 5. As shown in Fig. 5(a), the four O atoms of G3 coordinate to one Li ion to form a stable [Li(G3)]⁺ complex cation along with one [TFSA] anion to compensate for the positive charge in [Li(G3)][TFSA]. This structure is in good agreement with those reported in previous experimental and computational works.[50,58,59]

In contrast, based on the results of the correlation function ($g(r)$), a continuously ordered Li⁺ structure is formed in [Li(G3)][TFA] by coordinating both G3 and [TFA] anions (Fig. 5(b)). A similar coordination structure was confirmed in the solid crystal structure of a Li[TFA] and G4 mixture (Fig. S8, ESI†).[60] The peak positions of the Li⁺–Li⁺ correlation in [Li(G3)][TFA] (Fig. 4(a)) have a good agreement with the Li⁺–Li⁺ distances obtained from the crystal structure (see Table S5, ESI†). It is feasible that Li⁺–[TFA] anion aggregation and the continuously ordered Li⁺ structure observed in the crystal are maintained to some extent even in the liquid state.

3.4 Relationship between dynamic ion correlations and Li⁺ transference number

Here, we investigate the relationship between the dynamic ion correlations and the Li⁺ transference number. t_{Li}^{PP} can be defined using the Onsager transport coefficients as follows,[55,56]

$$t_{Li}^{PP} = \frac{\beta^2 - 4\alpha + 4\alpha^2}{4(1-\alpha)(\beta-1)} \quad (7)$$

$$\alpha = \frac{\sigma_{++}}{\sigma_{++} + \sigma_{--}}, \quad \beta = \frac{2\sigma_{+-}}{\sigma_{++} + \sigma_{--}} \quad (8)$$

If the ion motions are non-correlated ($\beta = 0$ for cation–anion correlations), as postulated in ideal solutions, t_{Li}^{PP} is equivalent to the parameters α and t_{Li}^{NMR}. In most cases of liquid electrolytes used in battery systems, however, ion correlations cannot be ignored. Thus, t_{Li}^{PP} is significantly varied by the interplay between the cation–cation and cation–anion cross-correlations.

In Fig. 6, t_{Li}^{PP} is simulated *versus* β for different α values. As predicted by eqn (7) (visualized in Fig. 6), the parameter α must be not less than 0.5 ($\alpha \geq 0.5$) in order to achieve $t_{Li}^{PP} = 1$. The parameter β is well explained by the strength of the cation–anion correlations represented by σ_{+-}. If the ion motions of the cation–anion are strongly anti-correlated, the value of β approaches −1.0. However, if strong correlations exist between cations and anions in the electrolytes, the β value approaches 1.0. Eqn (7) suggests that a t_{Li}^{PP} value of unity is attainable in the range of $0 \leq \beta \leq 1$. Consequently, the concentrated solution theory predicts the possibility of a single Li⁺ ion conducting liquid electrolyte, and there are several approaches within $\alpha \geq 0.5$ and $0 \leq \beta \leq 1$.

The α and β parameters for [Li(G3)][TFSA], [Li(G4)][BF₄], [Li(G3)][TfO], and [Li(G3)][TFA] are listed in Table 1. Furthermore, we illustrate the possible range of t_{Li}^{PP} as a function of β for different α values in Fig. 6, where the experimental values for [Li(glyme)]X are plotted. The Lewis basicity of the anions has an impact on both parameters α and β. According to our previous results,[20] the low value of α (0.25) for [Li(G3)][TFSA] chiefly stems from the strong anti-correlation of cation–cation motions. However, the value of α is close to 0.5 for [Li(G3)][TFA] and higher than that of [Li(G3)][TFSA]. Almost the same values of σ_{--} and σ_{++}, which are attributed to the coupled ion motions in the form of ion clusters, would result in $\alpha \to 0.5$ for [Li(G3)][TFA]. The parameter β predominantly depends on the Lewis basicity of the anion (eqn (8)). For [Li(G3)][TFSA], the anti-correlated ion motion of the cation–anion ($\sigma_{+-} < 0$) results in a largely negative value of β (−0.78). However, the β value gradually increases as the ion motion of the cation–anion shifts
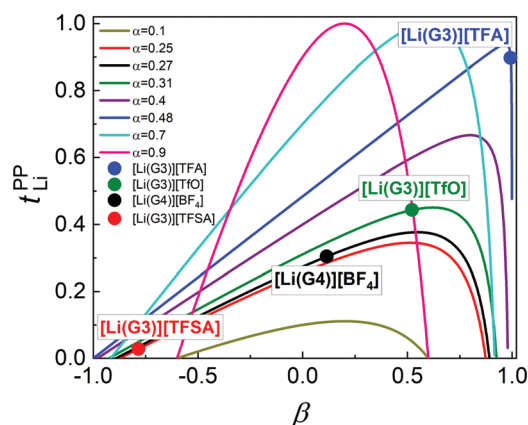

Fig. 6 Possible range of values for t_{Li}^{PP} as a function of β for different α values. The experimental data for [Li(G3)][TFSA], [Li(G4)][BF₄], [Li(G3)][TfO], and [Li(G3)][TFA] are plotted in the figure.

This journal is © the Owner Societies 2021

Phys. Chem. Chem. Phys., 2021, **23**, 2622–2629 | **2627**

Table 1 α and β values for the equimolar glyme–Li salt mixtures

Sample	α	β
[Li(G3)][TFSA][20]	0.25	−0.78
[Li(G3)][TfO]	0.31	0.52
[Li(G3)][TFA]	0.48	0.99
[Li(G4)][BF$_4$]	0.27	0.11

from anti-correlated ($\sigma_{+-} < 0$ for [Li(G3)][TFSA]) to nearly non-correlated ($\sigma_{+-} \approx 0$ for [Li(G4)][BF$_4$]) to correlated ($\sigma_{+-} > 0$ for [Li(G3)][TfO] and [Li(G3)][TFA]) with the increasing Lewis basicity of the anions. Therefore, the high t_{Li}^{PP} of 0.90 is found to be a consequence of the correlated ion motions of the cation–cation ($\alpha \approx 0.5$) and cation–anion ($\beta \approx 1$) in [Li(G3)][TFA].

For [Li(G3)][TFA], in which the high t_{Li}^{PP} is derived from strongly correlated ion motions ($\alpha \approx 0.5$, $\beta \approx 1$), the ionic conductivity becomes very low (0.096 mS cm^{-1}) because the large positive value of σ_{+-} negatively affects the ionic conductivity. Therefore, highly associating systems such as [Li(G3)][TFA] may not be adequate for simultaneously achieving high ionic conductivity and high t_{Li}^{PP}. In contrast, the previously studied SL-based molten Li salt solvates ([Li(SL)$_2$][TFSA] and [Li(SL)$_3$][TFSA]) showed a higher α value of $\sim$0.9 and a β parameter close to zero ($\beta = -0.18$ in the case of [Li(SL)$_3$][TFSA]), and exhibited a relatively high t_{Li}^{PP} value of $\sim$0.7 and ionic conductivity of 1.0 mS cm^{-1}.[20] Therefore, liquid electrolyte systems with non-correlated cation–anion ion motions ($\beta \approx 0$) and strongly correlated cation–cation motions ($\alpha \approx 1$) would be more appropriate for solving the trade-off problem between t_{Li}^{PP} and the ionic conductivity, as shown in Fig. 2.

4. Conclusions

The t_{Li}^{PP} behavior of [Li(glyme)]X was investigated as a function of ionicity and was enhanced with as the ionicity decreased (*i.e.*, as the Lewis basicity of the counter anions increased). However, a trade-off between the t_{Li}^{PP} and ionic conductivity was observed, which is similar to that of solid polymer electrolyte systems. The highest t_{Li}^{PP} of 0.93 was achieved for [Li(G4)][TFA], which had the lowest ionic conductivity of 0.083 mS cm^{-1}, whereas the lowest t_{Li}^{PP} value of 0.016 was found for [Li(G3)][FSA], with the highest ionic conductivity of 1.7 mS cm^{-1}. To clarify this trade-off, we studied the dynamic ion correlations for each electrolyte based on Roling and Bedrov's concentrated solution theory. The largely positive value of σ_{+-}/σ_{ion} was found to be the primary cause of the high t_{Li}^{PP} of [Li(G3)][TFA], and conversely, led to its low ionic conductivity.

We further explored the liquid structures of [Li(G3)][TFSA] and [Li(G3)][TFA] using a combination of HEXTS measurements and MD simulations. From the results of the Li$^+$–Li$^+$ and Li$^+$–anion pair correlation functions, it can be stated that Li$^+$ ions preferentially interact with G3 and form [Li(G3)]$^+$ complex cations in [Li(G3)][TFSA]. In contrast, Li$^+$ ions form an ordered structure through interaction with not only G3 molecules but also [TFA] anions in [Li(G3)][TFA]. These results strongly support the existence of ionic aggregates or ion

clusters of $[Li_x^+([TFA]^-)_y]^{(x-y)}$ as well as neutral ion pairs of Li–[TFA], as expected from the dynamic ion correlations.

We elucidated the Li$^+$ transference number as a function of the parameters α and β. [Li(glyme)]X with strongly associating anions, such as [Li(G3)][TFA], exhibited a high t_{Li}^{PP} with low ionic conductivity due to strongly correlated ion motions ($\alpha \approx 0.5$, $\beta \approx 1$). However, our analysis also suggested a possible approach to solving the trade-off using liquid electrolytes with non-correlated cation–anion ion motions ($\beta \approx 0$) and strongly correlated cation–cation motions ($\alpha \approx 1$). To develop an elaborate design principle for single-ion conducting liquid electrolytes with high ionic conductivity, future studies will focus on the achievement of $\alpha \approx 1$ and $\beta \approx 0$ values in low-viscosity liquid electrolyte systems.

Conflicts of interest

There are no conflicts to declare.

Acknowledgements

References

1 M. Doyle, T. F. Fuller and J. Newman, *Electrochim. Acta*, 1994, **39**, 2073–2081.

2 K. M. Diederichsen, E. J. McShane and B. D. McCloskey, *ACS Energy Lett.*, 2017, **2**, 2563–2575.

3 P. Barai, K. Higa and V. Srinivasan, *J. Electrochem. Soc.*, 2018, **165**, A2654–A2666.

4 H. Yoon, P. C. Howlett, A. S. Best, M. Forsyth and D. R. MacFarlane, *J. Electrochem. Soc.*, 2013, **160**, A1629–A1637.

5 Y. Yamada, K. Furukawa, K. Sodeyama, K. Kikuchi, M. Yaegashi, Y. Tateyama and A. Yamada, *J. Am. Chem. Soc.*, 2014, **136**, 5039–5046.

6 L. Suo, O. Borodin, T. Gao, M. Olguin, J. Ho, X. Fan, C. Luo, C. Wang and K. Xu, *Science*, 2015, **350**, 938.

7 J. Alvarado, M. A. Schroeder, M. Zhang, O. Borodin, E. Gobrogge, M. Olguin, M. S. Ding, M. Gobet, S. Greenbaum, Y. S. Meng and K. Xu, *Mater. Today*, 2018, **21**, 341–353.

8 M. Forsyth, H. Yoon, F. Chen, H. Zhu, D. R. MacFarlane, M. Armand and P. C. Howlett, *J. Phys. Chem. C*, 2016, **120**, 4276–4286.

9 K. Dokko, D. Watanabe, Y. Ugata, M. L. Thomas, S. Tsuzuki, W. Shinoda, K. Hashimoto, K. Ueno, Y. Umebayashi and M. Watanabe, *J. Phys. Chem. B*, 2018, **122**, 10736–10745.

10 X. Gao, F. Wu, A. Mariani and S. Passerini, *ChemSusChem*, 2019, **12**, 4185–4193.

11 E. R. Logan and J. R. Dahn, *Trends Chem.*, 2020, **2**, 354–366.

12 L. O. Valóen and J. N. Reimers, *J. Electrochem. Soc.*, 2005, **152**, A882.

2628 | *Phys. Chem. Chem. Phys.*, 2021, **23**, 2622–2629

This journal is © the Owner Societies 2021

13 S. Zugmann, M. Fleischmann, M. Amereller, R. M. Gschwind, H. D. Wiemhöfer and H. J. Gores, *Electrochim. Acta*, 2011, **56**, 3926–3933.

14 D. B. Shah, K. R. Olson, A. Karny, S. J. Mecham, J. M. DeSimone and N. P. Balsara, *J. Electrochem. Soc.*, 2017, **164**, A3511–A3517.

15 J. Popovic, D. Höfler, J. P. Melchior, A. Münchinger, B. List and J. Maier, *J. Phys. Chem. Lett.*, 2018, **9**, 5116–5120.

16 P. Ravn Sørensen and T. Jacobsen, *Electrochim. Acta*, 1982, **27**, 1671–1675.

17 M. Armand, *Solid State Ionics*, 1983, **9–10**, 745–754.

18 J. Evans, C. A. Vincent and P. G. Bruce, *Polymer*, 1987, **28**, 2324–2328.

19 Y. Tominaga, K. Yamazaki and V. Nanthana, *J. Electrochem. Soc.*, 2015, **162**, A3133–A3136.

20 K. Shigenobu, K. Dokko, M. Watanabe and K. Ueno, *Phys. Chem. Chem. Phys.*, 2020, **22**, 15214–15221.

21 K. Ueno, K. Yoshida, M. Tsuchiya, N. Tachikawa, K. Dokko and M. Watanabe, *J. Phys. Chem. B*, 2012, **116**, 11323–11331.

22 D. Dong, F. Sälzer, B. Roling and D. Bedrov, *Phys. Chem. Chem. Phys.*, 2018, **20**, 29174–29183.

23 D. B. Shah, H. Q. Nguyen, L. S. Grundy, K. R. Olson, S. J. Mecham, J. M. DeSimone and N. P. Balsara, *Phys. Chem. Chem. Phys.*, 2019, **21**, 7857–7866.

24 H. Moon, R. Tatara, T. Mandai, K. Ueno, K. Yoshida, N. Tachikawa, T. Yasuda, K. Dokko and M. Watanabe, *J. Phys. Chem. C*, 2014, **118**, 20246–20256.

25 S. Kohara, K. Suzuya, Y. Kashihara, N. Matsumoto, N. Umesaki and I. Sakai, *Nucl. Instrum. Methods Phys. Res., Sect. A*, 2001, **467–468**, 1030–1033.

26 S. Sakai, *National Laboratory for High Energy Physics*, Tsukuba, Japan, 1990.

27 D. T. Cromer, *J. Chem. Phys.*, 1969, **50**, 4857–4859.

28 J. H. Hubbell, W. J. Veigele, E. A. Briggs, R. T. Brown, D. T. Cromer and R. J. Howerton, *J. Phys. Chem. Ref. Data*, 1975, **4**, 471–538.

29 S. Nosé, *Mol. Phys.*, 1984, **52**, 255–268.

30 W. G. Hoover, *Phys. Rev. A: At., Mol., Opt. Phys.*, 1985, **31**, 1695–1697.

31 J. N. Canongia Lopes and A. A. H. Pádua, *J. Phys. Chem. B*, 2004, **108**, 16893–16898.

32 W. D. Cornell, P. Cieplak, C. I. Bayly, I. R. Gould, K. M. Merz, D. M. Ferguson, D. C. Spellmeyer, T. Fox, J. W. Caldwell and P. A. Kollman, *J. Am. Chem. Soc.*, 1995, **117**, 5179–5197.

33 W. L. Jorgensen, D. S. Maxwell and J. Tirado-Rives, *J. Am. Chem. Soc.*, 1996, **118**, 11225–11236.

34 E. K. Watkins and W. L. Jorgensen, *J. Phys. Chem. A*, 2001, **105**, 4118–4125.

35 S. Saito, H. Watanabe, K. Ueno, T. Mandai, S. Seki, S. Tsuzuki, Y. Kameda, K. Dokko, M. Watanabe and Y. Umebayashi, *J. Phys. Chem. B*, 2016, **120**, 3378–3387.

36 J.-C. Soetens, C. Millot and B. Maigret, *J. Phys. Chem. A*, 1998, **102**, 1055–1061.

37 C. M. Breneman and K. B. Wiberg, *J. Comput. Chem.*, 1990, **11**, 361–373.

38 Y. Kamiyama, M. Shibata, R. Kanzaki and K. Fujii, *Phys. Chem. Chem. Phys.*, 2020, **22**, 5561–5567.

39 K. Hayamizu, Y. Aihara, S. Arai and C. G. Martinez, *J. Phys. Chem. B*, 1999, **103**, 519–524.

40 Y. Ugata, R. Tatara, K. Ueno, K. Dokko and M. Watanabe, *J. Chem. Phys.*, 2020, **152**, 104502.

41 P. G. Bruce, J. Evans and C. A. Vincent, *Solid State Ionics*, 1988, **28–30**, 918–922.

42 M. Watanabe, S. Nagano, K. Sanui and N. Ogata, *Solid State Ionics*, 1988, **28–30**, 911–917.

43 M. D. Galluzzo, J. A. Maslyn, D. B. Shah and N. P. Balsara, *J. Chem. Phys.*, 2019, **151**, 020901.

44 D. R. MacFarlane, M. Forsyth, E. I. Izgorodina, A. P. Abbott, G. Annat and K. Fraser, *Phys. Chem. Chem. Phys.*, 2009, **11**, 4962–4967.

45 K. R. Harris, *J. Phys. Chem. B*, 2010, **114**, 9572–9577.

46 K. Ueno, H. Tokuda and M. Watanabe, *Phys. Chem. Chem. Phys.*, 2010, **12**, 1649–1658.

47 H. K. Kashyap, H. V. R. Annapureddy, F. O. Raineri and C. J. Margulis, *J. Phys. Chem. B*, 2011, **115**, 13212–13221.

48 C. Austen Angell, Y. Ansari and Z. Zhao, *Faraday Discuss.*, 2012, **154**, 9–27.

49 W. A. Henderson, *J. Phys. Chem. B*, 2006, **110**, 13177–13183.

50 W. Shinoda, Y. Hatanaka, M. Hirakawa, S. Okazaki, S. Tsuzuki, K. Ueno and M. Watanabe, *J. Chem. Phys.*, 2018, **148**, 193809.

51 L. A. Woolf, *J. Phys. Chem.*, 1978, **82**, 959–962.

52 L. A. Woolf and K. R. Harris, *J. Chem. Soc., Faraday Trans. 1*, 1978, **74**, 933–947.

53 D. M. Pesko, K. Timachova, R. Bhattacharya, M. C. Smith, I. Villaluenga, J. Newman and N. P. Balsara, *J. Electrochem. Soc.*, 2017, **164**, E3569–E3575.

54 I. Villaluenga, D. M. Pesko, K. Timachova, Z. Feng, J. Newman, V. Srinivasan and N. P. Balsara, *J. Electrochem. Soc.*, 2018, **165**, A2766–A2773.

55 F. Wohde, M. Balabajew and B. Roling, *J. Electrochem. Soc.*, 2016, **163**, A714–A721.

56 N. M. Vargas-Barbosa and B. Roling, *ChemElectroChem*, 2020, **7**, 367–385.

57 K. Fujii, M. Matsugami, K. Ueno, K. Ohara, M. Sogawa, T. Utsunomiya and M. Morita, *J. Phys. Chem. C*, 2017, **121**, 22720–22726.

58 S. Tsuzuki, W. Shinoda, M. Matsugami, Y. Umebayashi, K. Ueno, T. Mandai, S. Seki, K. Dokko and M. Watanabe, *Phys. Chem. Chem. Phys.*, 2015, **17**, 126–129.

59 K. Ueno, R. Tatara, S. Tsuzuki, S. Saito, H. Doi, K. Yoshida, T. Mandai, M. Matsugami, Y. Umebayashi, K. Dokko and M. Watanabe, *Phys. Chem. Chem. Phys.*, 2015, **17**, 8248–8257.

60 W. A. Henderson, N. R. Brooks and V. G. Young, *Chem. Mater.*, 2003, **15**, 4685–4690.

This journal is © the Owner Societies 2021

Phys. Chem. Chem. Phys., 2021, **23**, 2622–2629 | **2629**